

AperTO - Archivio Istituzionale Open Access dell'Università di Torino

## On the high-temperature phase of barbituric acid

### This is the author's manuscript

*Original Citation:*

*Availability:*

This version is available <http://hdl.handle.net/2318/105394> since 2016-10-18T22:36:58Z

*Published version:*

DOI:10.1039/c2ce06636j

*Terms of use:*

Open Access

Anyone can freely access the full text of works made available as "Open Access". Works made available under a Creative Commons license can be used according to the terms and conditions of said license. Use of all other works requires consent of the right holder (author or publisher) if not exempted from copyright protection by the applicable law.

(Article begins on next page)



# UNIVERSITÀ DEGLI STUDI DI TORINO

***This is an author version of the contribution published on:***

*Questa è la versione dell'autore dell'opera:*

*CrystEngComm, 2012, 14, 3046, DOI: 10.1039/c2ce06636j*

***The definitive version is available at:***

*La versione definitiva è disponibile alla URL:*

*<http://dx.doi.org/10.1039/c2ce06636j>*

# On the high-temperature phase of barbituric acid

Daniel M. Többens<sup>\*a</sup>, Jürgen Glinneman<sup>b</sup>, Michele R. Chierotti<sup>c</sup>, Jacco van de Streek<sup>d</sup>, Denis Sheptyakov<sup>e</sup>

The crystal structure of the high-temperature phase (HT-form or form III) of barbituric acid has been solved from X-ray powder diffraction data. It was found to be monoclinic, space group  $C2/c$ ,  $a = 8.5302(3) \text{ \AA}$ ,  $b = 6.8167(3) \text{ \AA}$ ,  $c = 9.3304(4) \text{ \AA}$ ,  $\beta = 89.865(2)^\circ$ , volume =  $542.54(4) \text{ \AA}^3$  at  $T = 236(1)^\circ\text{C}$ . The crystal structure is closely related to the also monoclinic structure of form II. A combined Rietveld refinement of X-ray and neutron powder diffraction data revealed fine details of the disorder aspects of the structure.  $^1\text{H}$  variable temperature and  $^{13}\text{C}$  MAS solid-state NMR confirmed those and proved the dynamic nature of the rotational disorder of the molecules. Energy optimizations of ordered subgroup structures with dispersion-corrected DFT gave insights into the underlying reason for the disorder. The reorientation of the unique 2-fold symmetry axis at the II  $\rightarrow$  HT phase transition derives from both the anisotropy of the hydrogen bonds and the resulting anisotropy of the thermal rotational disorder. The unusual thermal expansion behavior of form II also finds its explanation in the incipient disorder.

## Introduction

Barbituric acid [BAc, 2,4,6(1H,3H,5H)-pyrimidinetrione],  $\text{C}_4\text{H}_4\text{N}_2\text{O}_3$  (figure 1) was first synthesized in 1863 by Adolf von Baeyer.<sup>1</sup> It is used as precursor in the synthesis of numerous compounds such as polymers,<sup>2</sup> pigments,<sup>3</sup> dyes,<sup>4</sup> and Vitamin B2.<sup>5</sup> In addition, while itself pharmacologically inactive, it is the lead structure of the 5,5-substituted barbiturates, the dominating group of sedative/hypnotic drugs during the first half of the 20<sup>th</sup> century. The importance of BAc is reflected in numerous research papers. Nonetheless, while the crystal structure of form I (the “Bolton” form) of barbituric acid has been known since 1963,<sup>6</sup> it took until 2004 to discover a second polymorph.<sup>7</sup> This form II is monoclinic with two independent molecules in the asymmetric unit, forming almost planar hydrogen-bonded sheets. It soon became obvious that commercially available barbituric acid consists of this form II,<sup>8</sup> rather than of the metastable form I described in the earlier literature. For these reasons, form II has been considered the most stable phase, until form IV was

discovered in 2008.<sup>9</sup> While the former two polymorphs consist of molecules in the keto tautomeric form (figure 1), this new polymorph, obtained by grinding form II, consists of molecules in the enol form stabilized by a higher number of hydrogen bonds as shown recently by neutron powder diffraction and  $^1\text{H}$  MAS experiments.<sup>10</sup>

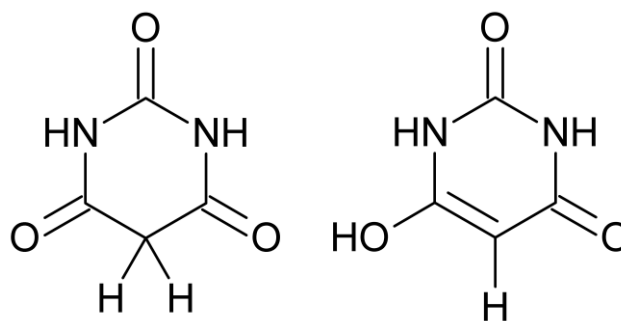


**Fig. 1** The tautomeric forms of the barbituric acid molecule (left keto, right enol).

The existence of a high-temperature phase (form III or HT-form) has been reported recently by Roux *et al.*,<sup>11</sup> and was characterized in detail by Zenciri *et al.*<sup>12</sup> However, none of the previous attempts to solve its crystal structure were successful. Zenciri *et al.*<sup>12</sup> noticed that the X-ray powder diffraction (XRPD) pattern they obtained was different from the diffractogram reported by Roux *et al.*, with some reflections matching those obtained from a thermally decomposed product. They proposed a monoclinic unit cell with space group  $P2_1/n$ , four formula units per unit cell and lattice parameters  $a = 9.293(4) \text{ \AA}$ ,  $b = 6.765(3) \text{ \AA}$ ,  $c = 8.185(5) \text{ \AA}$ ,  $\beta = 91.75(2)^\circ$ ,  $V = 514.34(2) \text{ \AA}^3$ . However, structure solution could not be achieved. The only insight into the structure of the HT-form came from Raman- and IR-spectra, which were shown to be closely related to those of

<sup>a</sup>Institute of Mineralogy and Petrography, University of Innsbruck, Innrain 52, A-6020, Austria, now Helmholtz-Zentrum Berlin für Materialien und Energie, Hahn-Meitner-Platz 1, D-14109 Berlin, Germany

<sup>b</sup>Institute of Inorganic and Analytical Chemistry, University of Frankfurt, Max-von-Laue-Str. 7, D-60438 Frankfurt am Main, Germany

<sup>c</sup>Department of Chemistry I.F.M. and NIS Centre of Excellence, University of Turin, Via Pietro Giuria 7, I-10125 Turin, Italy

<sup>d</sup>Avant-garde Materials Simulation, Merzhauser Str. 177, D-79100 Freiburg im Breisgau, Germany

<sup>e</sup>Laboratory for Neutron Scattering, Paul Scherrer Institut, CH-5232 Villigen PSI, Switzerland

† Electronic Supplementary Information (ESI) available: Crystallographic information file of experimental and energy optimized structures, experimental structure and bond parameters, X-ray and neutron powder diffraction data, figure showing peaks from phase impurities, experimental and calculated  $^1\text{H}$  chemical shift tensors and shielding anisotropy, lattice parameters as a function of temperature

form II<sup>12</sup>. The two forms therefore are expected to have similar structures, in particular the same keto tautomerization of the molecule.

## Experimental section

### Materials

Barbituric acid p.A. (Fluka, Aldrich) was used for the experiments. The material was confirmed as pure form II by X-ray powder diffraction.

Deuterated BAC form II was obtained by solving commercial BAC in D<sub>2</sub>O. The formation of the HT-form was observed by XRPD. Nonetheless, during the neutron diffraction experiments the compound always decomposed before the HT-form could be measured. Neutron powder diffraction data of the HT-phase were thus obtained from <sup>1</sup>H samples.

### X-ray powder diffraction

XRPD data for structure determination and thermal expansion analysis were collected on a Stoe STADI MP diffractometer, equipped with an asymmetric primary beam Ge(111) monochromator (yielding a strictly monochromatic CuK $\alpha_1$ -radiation), a Mythen.2k microstrip detector, and a 0.65.LT furnace using a capillary of 0.5 mm diameter for the sample. The temperature stability and gradient of the furnace was established to be as low as  $\pm 0.5$  °C, and the temperature scale was calibrated with phase transformations of NH<sub>4</sub>NO<sub>3</sub>, KNO<sub>3</sub>, and KCl to an accuracy < 1 °C. External calibration of the peak positions with Silicon SRM 640a showed reproducibility down to the resolution-mandated detection limit and positional accuracy of the peaks of  $\pm 0.002^\circ$ .

Data for the determination of thermal expansion and phase transition temperatures were measured isothermally, with a ramp rate of 1 °C/min between data collections. Due to the long individual data collection times (110 min and 20 min) the effective heating rate is dominated by the size of the temperature steps. At effective changes below 5 °C/h transition temperatures were found to be independent of the heating rate. At higher rates of heating and cooling, the transition temperature shifts. The lattice parameters are not influenced by the rates of temperature change. Data reported in here (figures 7, 8, S5, table S6) result from measurements done at heating rates of 0.5 and 3 °C/h, and cooling rates of 3 and 6 °C/h. XRPD data for the structure determination were taken at a temperature of 236(1) °C, which was approached carefully at a heating rate of 10 °C/min up to 220 °C, and 4 °C/h up to 236 °C. A powder diffraction pattern of the pure decomposition products was obtained by heating the sample up to 250 °C and subsequent cooling to 236 °C.

### Neutron powder diffraction

Neutron diffraction data were obtained with the high-resolution neutron diffractometer HRPT<sup>13</sup> at PSI with the neutron wavelength  $\lambda = 1.886(1)$  Å in high-intensity mode. A radiation-type furnace was used, which was judged to have the lowest temperature gradient on the sample. For further reduction of the gradient, the sample height was limited to 4 cm. For the heating runs the sample was heated up to 230 °C at a rate of 1 °C/min, and subsequently up to 240 °C at a rate

of 0.2 °C/min. Due to an inevitable temperature gradient of unknown strength and slow equilibration of the large furnace, the temperature readout of the neutron diffraction experiment has a higher uncertainty. Based on the monoclinic angle of an independent refinement of the neutron diffraction lattice parameters, the temperature was determined as 236(2) °C, the same as in the XRPD experiments. Decomposition of the sample still occurred within a short time interval. This severely limited the intensity of the neutron diffraction data.

### Structure solution and refinement

Computer programs utilized in the structure determination and refinement process are *WinXPow*<sup>14</sup> (peak fitting), *Crysfire*<sup>15</sup> and *Chekcen*<sup>16</sup> (indexing), *Fox* SVN 20060227<sup>17</sup> (structure determination by simulated annealing), *Fullprof.2k* 4.80<sup>18</sup> (LeBail- and Rietveld refinement). For the structure solution process, the molecule was modeled as rigid body. The only free internal parameter of the molecular model was the out-of-plane angle of the CH<sub>2</sub>-group, which can be either in a flat or in an envelope conformation in BAC. Thermal displacement was treated with the TLS approach,<sup>19</sup> allowing only translational and rotational displacements of the whole molecule. For the final refinement after selection of the correct model, soft restraints based on the energy-optimized geometry of form II were applied to the bond distances and angles of the non-hydrogen atoms. Hydrogen atoms were treated as riding atoms in geometrically optimized position. Atoms for which refinement of isotropic displacement resulted in large values were refined with anisotropic displacement parameters. Careful selection of the refineable terms had to be applied in order to avoid unphysical solutions. The anisotropy of atomic displacement thus should be interpreted very cautiously. X-ray and neutron powder diffraction data were refined simultaneously with the same structure model.

Details of the data collection, structure refinement, and residuals of the final model are given in table 1. The powder diffraction pattern of X-rays and neutrons and the corresponding Rietveld fits of the final model are shown in figure 2.

### Solid-state NMR

Solid-state NMR spectra were acquired on a Bruker Avance III 500 spectrometer with a wide bore 11.7 T magnet operating at 500.13 and 125.77 MHz for <sup>1</sup>H and <sup>13</sup>C, respectively. The sample was packed in a 7 mm outer diameter ZrO<sub>2</sub> rotor and spun at 4 kHz in a high-temperature probe. <sup>13</sup>C Magic Angle Spinning (MAS) high power decoupling spectra were collected using delay times of 20 s, acquisition times of 0.02 s and a <sup>13</sup>C 90° pulse of 7.0  $\mu$ s. A single-pulse experiment was used to acquire <sup>1</sup>H MAS spectra with delay times of 5 s, acquisition times of 0.04 s and a <sup>1</sup>H 90° pulse of 4.0  $\mu$ s. Temperature calibration was performed using lead nitrate as <sup>207</sup>Pb MAS NMR chemical shift thermometer. All chemical shifts are reported using the  $\delta$  scale and are externally referenced to adamantane at 1.87 ppm (<sup>1</sup>H) and 38.48 ppm (<sup>13</sup>C). Chemical shift tensors and shielding anisotropies were extracted by computer simulation of the spinning sideband patterns using the HBA program<sup>21</sup>

**Table 1** Experimental diffraction conditions and joined Rietveld analysis

Radiation	X-ray, Cu K $\alpha_1$	Neutrons
Sample & phase	Barbituric acid (BAC), HT-form	
Formula		C <sub>4</sub> H <sub>4</sub> N <sub>2</sub> O <sub>3</sub>
Formula mass		128.09 g/mol
Temperature	236(1) °C	236(2) °C
Wavelength	1.540593 Å	1.886(1) Å
Instrument	STOE Stadi MP with Mythen.2k	PSI HRPT / SINQ
Experimental geometry	Capillary Ø = 0.5 mm, focusing beam	Vanadium tube, Ø = 6 mm
Density (calculated)		1.17 g/cm <sup>3</sup>
Absorption coefficient $\mu_R$ =	0.18	0.33
Crystal system		monoclinic
Space group		C2/c (15)
<i>a</i>		8.5302(3) Å
<i>b</i>		6.8167(3) Å
<i>c</i>		9.3304(4) Å
$\beta$		89.865(2)°
Volume		542.54(4) Å <sup>3</sup>
Z / Z'	4 / 1 (disordered, occupation factors 0.5)	
2 $\theta$ range for data collection	3.0 – 82.2°	5.0 – 160.0°
Reflections collected	911	324
Independent reflections	167	149
Refinement method	Soft restraints, partially anisotropic atomic displacements, simultaneous refinement of X-ray and neutron diffraction patterns	
Profile / Structural parameters	79 / 29	
Goodness of fit (on $y_{\text{obs}}$ )	2.13	1.17
weighted pattern residual <i>Rwp</i>	0.054	0.017
Bragg <i>R</i> -factor	0.023	0.151
Bérar's e.s.d. correction factor <sup>20</sup>		2.2

based on the algorithm developed by Herzfeld and Berger<sup>22</sup>. The principal tensor components are reported according to the standard convention<sup>23</sup> where  $\delta_{11} \geq \delta_{22} \geq \delta_{33}$  and the shielding anisotropy is defined as  $\Delta\sigma = \sigma_{33} - (\sigma_{11} + \sigma_{22})/2$  with  $\sigma_{11} \leq \sigma_{22} \leq \sigma_{33}$  and  $\delta_{ii} = -\sigma_{ii}$ .

### NMR computational details

Full geometry optimization in the gas phase was performed by means of DFT with the Gaussian09 program,<sup>24</sup> at the B3LYP/6-311++G-(d,p) level. The NMR shielding parameters were calculated starting from the optimized geometry within the gauge-including atomic orbital (GIAO) method at the B3LYP/6-311++G-(d,p) level. The <sup>1</sup>H chemical shifts were referred to the computed shielding for TMS optimized at B3LYP/6-311++G(d,p) (absolute isotropic constant shielding values of 31.9698) and calculated according to the equation  $\delta_s = 31.9698 - \sigma_s$  (where the subscript “s” refers to the sample).

### Computational parameters of DFT-D calculations

The crystal structures were optimized with dispersion-corrected Density Functional Theory (DFT-D) with the program GRACE,<sup>25</sup> which uses VASP 4.6<sup>26,27,28</sup> for single-point pure DFT calculations. The Generalized Gradient

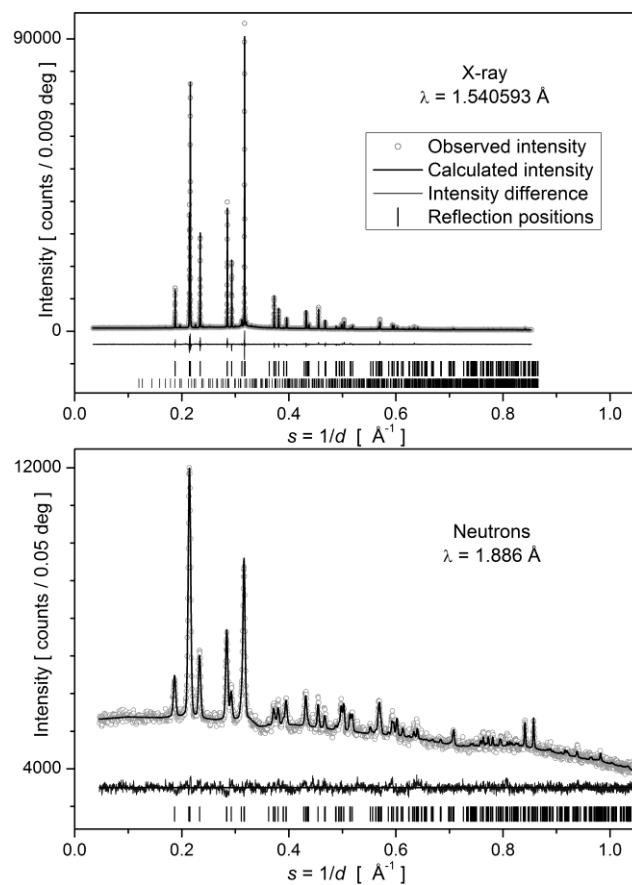


**Fig. 2** Rietveld refined of X-ray (top) and neutron (bottom) powder diffraction patterns of the HT-form of BAC, using a common  $s = 1/d = 2\sin\theta/\lambda$  scale. The bottom row of reflection positions shown for the XRPD is from the minor fraction of remaining form II, giving rise to diffraction peaks barely visible on this intensity scale.

Approximation (GGA) with the BLYP<sup>29,30</sup> exchange-correlation functional was used, with standard projector-augmented wave (PAW) potentials. The plane-wave cut-off energy was 520 eV, the *k*-point spacing was approximately 0.7 Å<sup>-1</sup>. The latest dispersion correction by Grimme<sup>31</sup> was used. The calculations were run with variable lattice parameters with the space-group symmetry imposed.

### Crystal structure of high-temperature form

At temperatures above 233–237 °C BAC form II transforms into the HT-form. This form can be preserved for short times at lower temperatures, depending on the cooling rate, but could not be preserved at ambient temperature.

### Dynamic nature from solid-state NMR

<sup>13</sup>C MAS solid-state NMR measurements acquired at 233 °C (figure 3 comparison with form II and table 2) agree with the presence of keto molecules in the structure as highlighted by the C5 signal at 40.2 ppm typical of CH<sub>2</sub> rather than CH groups<sup>32</sup> (see figure 1 for atom numbers). The doublet (41.1 and 39.1 ppm) characterizing the spectrum of form II and resulting from the CH<sub>2</sub> group of the two independent

molecules present in this form<sup>9</sup>, merge into a singlet in HT-form. The other peaks, 151.9 and 168.4 ppm attributed to C2 and C4/C6 respectively, indicate the presence of only one independent molecule in the unit cell. Very narrow signals (line widths around 90-95 Hz) in HT-form suggest the presence of extensive motions of the molecules. <sup>1</sup>H MAS variable temperature (VT) spectra (figure 4) confirm the dynamic nature of the polymorph adding insights on the II → HT phase transition. Until 222 °C the <sup>1</sup>H spectrum does not change, showing two very broad resonances around 10.9 (NH) and 2.6 (CH<sub>2</sub>) ppm with many spinning sidebands arising from an inadequate average of the strong <sup>1</sup>H-<sup>1</sup>H dipolar interaction as expected for slow spinning speed <sup>1</sup>H spectra (4 kHz). Interestingly, when increasing the temperature to 231 °C two narrow signals appear at 4.4 and 9.6 ppm (line width of 270 and 316 Hz, respectively) with sharp spinning sidebands forming an asymmetric pattern typical of chemical shift anisotropy (CSA) rather than dipolar interaction (which, instead, is symmetric).<sup>33</sup> This phenomenon can be explained with the presence of a fast anisotropic molecular rotation able to average almost completely the <sup>1</sup>H-<sup>1</sup>H dipolar interaction while the CSA, although smaller, is not efficiently affected. However, <sup>1</sup>H chemical shift tensor and shielding anisotropy values (table S1, supporting information) indicate that the dipolar interaction still shapes the sideband pattern.<sup>23</sup> Indeed, the obtained experimental shielding anisotropy values (around 17-19 ppm) are much higher than those computed on BAc in gas phase (around 4.8 for CH<sub>2</sub> and 4.2 for NH ppm, table S1 in the supporting information), which agree with values around 1-13 ppm reported in literature for other molecules.<sup>34-37</sup>

By leaving the sample at 233 °C for some minute the spinning sidebands decrease until completely disappearing after 45 min. At this point the <sup>1</sup>H spectrum is characterized by two resonances at 5.0 and 10.5 ppm, with other broad signals assigned to decomposition products. The absence of spinning sidebands indicates that HT-form is characterized by a high mobility, on the NMR time scale, able to average both CSA and dipolar interactions.

### Disordered structure from powder diffraction

Finding the correct unit cell of HT-form from diffraction data is hampered by the fact that at temperatures above 242 °C BAc decomposes rapidly. In most cases, traces of decomposition products are found at lower temperatures already, even below the II → HT transformation temperature. The additional diffraction peaks from the decomposition products can lead to false unit cells or mask systematic extinctions. To circumvent this problem, an XRPD of the pure decomposition products was taken at a temperature of 236(1) °C and, after suitable scaling, stripped from the XRPD of HT-form (figure S2, supporting information). In the same vein, a remaining fraction of 2.3(1) % of form II was treated as a minor fraction during the Rietveld refinement, and the corresponding peaks were excluded from the indexing process.

All remaining peaks could be indexed with a monoclinic unit cell, volume = 542.54(4) Å<sup>3</sup>, *a* = 8.5302(3) Å, *b* =

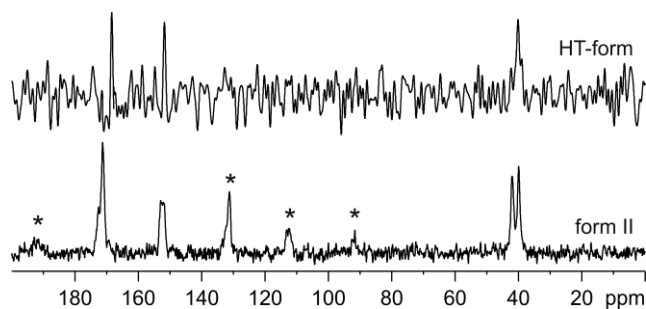


**Fig. 3** Comparison between <sup>13</sup>C solid-state NMR spectra of BAc form II (bottom; CPMAS spectrum at 27 °C, 32 scans and spinning speed of 5 kHz) and HT-form (top; MAS spectrum at 233 °C, 16 scans and spinning speed of 4 kHz). Asterisks denote spinning sidebands.

**Table 2** <sup>1</sup>H and <sup>13</sup>C chemical shifts (ppm) with assignments for BAc HT-form.

<sup>1</sup> H δ	hydrogen atom	<sup>13</sup> C δ	carbon atom
10.5	H1/H3	151.9	C2
5.0	H5	168.4	C4/C6
		40.2	C5

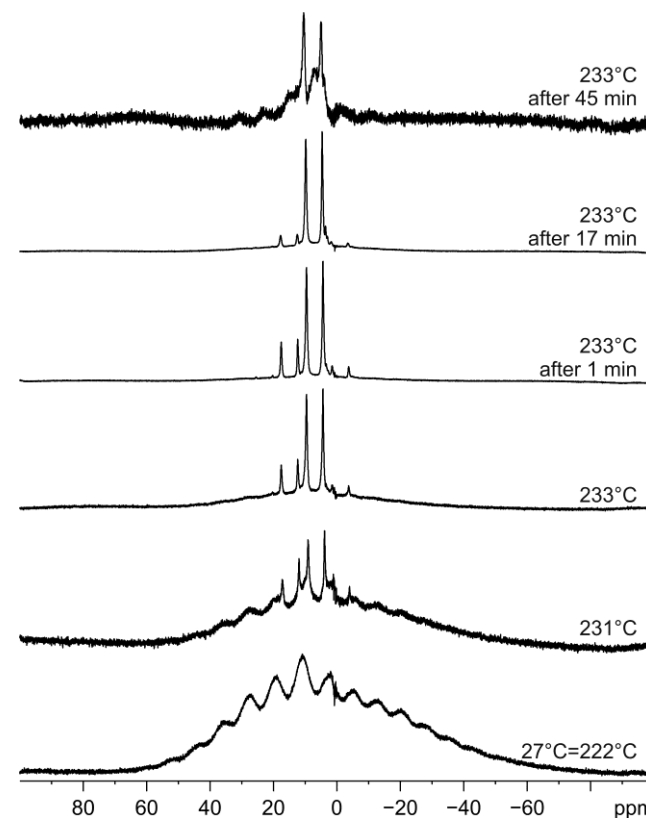


**Fig. 4** <sup>1</sup>H VT MAS spectra of BAc form II from 27 °C to 233 °C acquired with a spinning speed of 4 kHz and 16 scans each.

6.8167(3) Å, *c* = 9.3304(4) Å,  $\beta$  = 89.865(2) °. From the systematic reflection conditions the extinction symbol *C1c1* is assured, allowing either space group *Cc* or *C2/c*. Structure solution was possible in both symmetries. In both space groups, structure determination gave very similar results, with the molecules arranged around the 4*e* Wyckoff position in *C2/c* and a very similar arrangement in *Cc* with general

positions. The molecule appears to be in planar conformation. This is in contrast to form II, where the molecule appears in two different conformations, planar and envelope. However, in HT-form the CH<sub>2</sub>-moiety exhibits strong anisotropic thermal displacement normal to the plane of the molecule (figure 5). This reveals local envelope conformations, with disordered directions of the envelope. The DFT optimization of the ordered *Cc* model confirms this interpretation (table 4). Given the dynamic nature of the phase it is likely that this disorder is dynamic, too.

Similar to form II, the molecules form layers with each molecule surrounded by four neighbors. However, a major difference arises from the interaction of the internal symmetry of the molecules, *2/m* in planar conformation, and the site symmetry. In *Cc* any orientation of the molecule is possible in a fully ordered structure, since the site does not impose symmetry beyond identity; no special Wyckoff positions exist in this space group. In *C2/c*, the crystallographic site symmetry is 2, thus only congruent orientation of the molecules would result in a fully ordered structure. Other orientations result in disorder, with two differently oriented molecules superimposed with 1:1 frequency. These different orientations of the molecule inside the structure exchange the CH<sub>2</sub> moiety with an NH moiety. Since both moieties hold eight electrons each, the resulting changes in the electronic density are too small to be clearly recognizable in an XRPD pattern of a high-temperature phase with significant thermal displacement of the atoms. For neutron diffraction, the scattering factor of hydrogen is higher, and the difference in the scattering factors of N and C is larger ( $b_c(\text{H}) = -3.739(1)$ ,  $b_c(\text{C}) = 6.646(1)$ ,  $b_c(\text{N}) = 9.36(2)$ <sup>38</sup>), resulting in strong differences between CH<sub>2</sub> and NH. Simultaneous Rietveld refinement of neutron and X-ray powder diffraction data thus allowed discrimination of the two structural models. The same holds for other types of disorder that would place carbon in

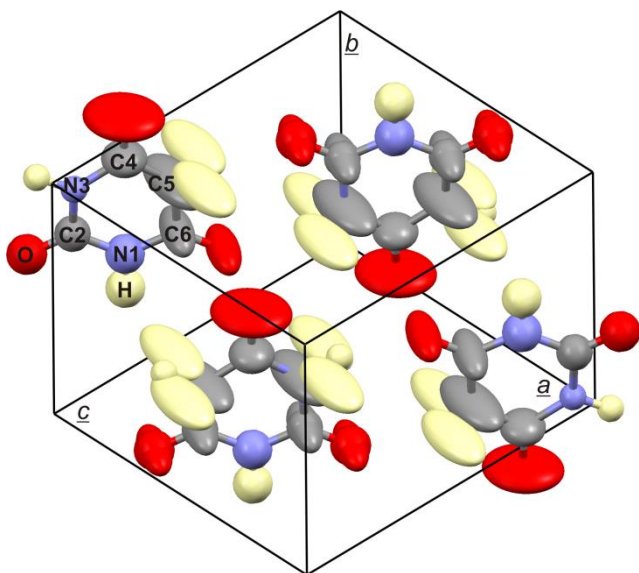


**Fig. 5** The structure of HT-BAC from joined refinement of X-ray and neutron powder diffraction data. At two sites the 2-fold orientational disorder of the molecules is not depicted for clarity. Atoms are represented by 50%-probability ellipsoids. Note the high displacement factors close to the flexible region of the molecule.

the site occupied by N1. It was found that HT-form of BAC is disordered in space group *C2/c* (figure 5, tables S3 and S4 supporting information). The residuals for this model are significantly lower than for any ordered arrangement either in *C2/c* or *Cc*, even if the molecule is placed on two independent split positions with 50% occupation each in *Cc*. This demonstrated conclusively that the structural disorder is not just a displacement of the molecules, but a rotation exchanging the CH<sub>2</sub> and a NH moiety, which is in agreement with the anisotropic rotation detected by <sup>1</sup>H VT MAS spectra. In light of the mobility observed from <sup>1</sup>H MAS, the dynamic character of this disorder is obvious. In this regard one has to take into account the relevant millisecond time scale of the NMR technique. The implications this dynamic disorder has for the structure, in particular the formation of the hydrogen bond network, are discussed in the following.

## The hydrogen bond network

In both previously known crystal structures composed of keto-BAC molecules, form I and form II, each BAC molecule forms four N-H···O hydrogen bonds. Each individual molecule has two N-H moieties acting as donor, and two of the three carbonyl groups act as acceptor for the neighboring molecule NH groups. The third oxygen remains unpaired. The difference among the arrangements is in the way these bonds are distributed over the neighbors.

In form II (figure 6), one chain of relatively straight hydrogen bonds lies along the direction  $[10\bar{1}]$ . ( $\text{C}=\text{O}\cdots\text{N}$  angles of

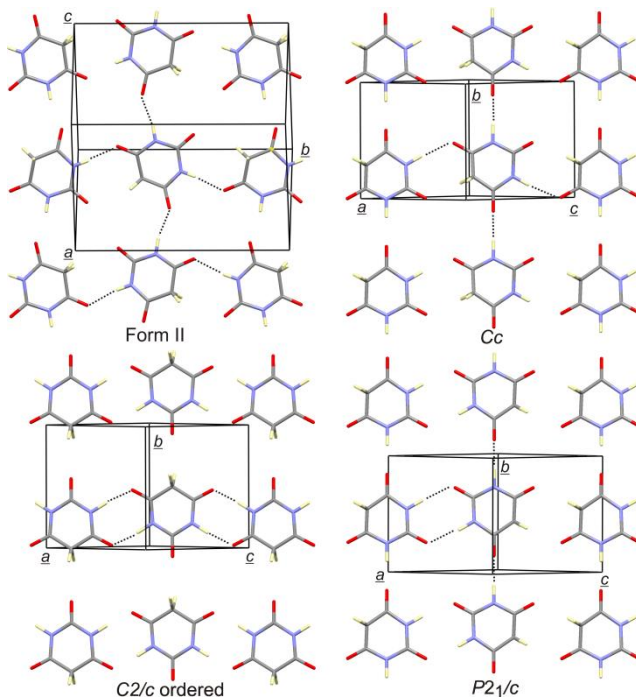


**Fig. 6** Hydrogen bond networks: N-H···O hydrogen bonds within a layer of form II (upper left), HT-form described as ordered in subgroup *Cc* (upper right) and *P2<sub>1</sub>/c* (lower right), and a hypothetical ordered arrangement in space group *C2/c*. In all cases, each molecule forms 4 N-H···O bonds and 2 C-H···O contacts, but with different distribution over the four neighbors. The real, disordered structure of HT-form, also in space group *C2/c*, is not shown. Note the different unique monoclinic axis and unit cell in form II.

**Table 3** Geometry of energy optimized structures and corresponding experimental values

Structure	V / Å <sup>3</sup>	a / Å	b / Å	c / Å	β / deg
Form I at 150 K <sup>7</sup>	527.1(2)	6.731(2)	14.029(4)	6.231(2)	116.37(1)
Form I, <i>ab initio</i>	538.3	6.790	14.119	6.264	116.315
Form II at 150 K <sup>7</sup>	987.4(1) (=2 x 493.7)	8.083(1)	12.583(2)	9.764(1)	96.15(1)
Form II, <i>ab initio</i>	1002.1 (= 2 x 501.0)	8.108	12. 97	9.877	96.55
HT-form at 236 °C	542.5(4)	8.530(4)	6.817(3)	9.330(4)	89.86(2)
HT-form quenched at 20 °C	517.6(25)	8.191(7)	6.800(4)	9.298(7)	91.6(3)
HT-form, <i>Cc</i> type, <i>ab initio</i>	508.9	8.056	6.823	9.264	92.11
HT-form, <i>P2<sub>1</sub>/c</i> type, <i>ab initio</i>	514.1	8.218	6.870	9.124	93.66
HT-form, <i>C2/c</i> ordered, <i>ab initio</i>	547.3	8.149	7.245	9.272	91.17

150.2° and 150.9°, structure at 150 K <sup>7</sup>). The other chain runs orthogonal to the first one, along direction [010], and is composed of bent bonds, with C=O...N angles of 131.9° and 134.4°. In HT-form, the overall arrangement of the molecules is very similar. However, the chain of straight hydrogen bonds, with symmetry-enforced bond angles of 180°, lies along the [010] direction. This reorientation of the monoclinic axis destroys the symmetry relation between HT-form and form II structures.

The chain of bent bonds in HT-form consequently lies along the  $[10\bar{1}]$  direction, with a C=O...N angle of 128.1°. For this direction, the presence of orientational disorder in the structure of HT-form hinders the analysis of the nature of the hydrogen bonding. In particular, the 2-fold axis of the crystal structure repositions some of the N–H moieties that act as donors in the formation of hydrogen bonds. However, any structural disorder is only a result of averaging, either over multiple unit cells or, in the case of dynamic disorder, over time. At any particular point, only a discrete distribution exists. It is therefore expedient to look at the possible ordered structures underlying the disordered average. In this case, the observed disorder is the result of the 2-fold axis in the crystal symmetry (and *vice versa*). The most straightforward way to resolve the disorder is thus a reduction of the symmetry (figure 6). We restrict the analysis to the maximal subgroups of index 2 of space group *C2/c*. There are seven of these: *Cc*, *P2<sub>1</sub>/n*, *P2<sub>1</sub>/c*, *P1*, *C2*, *P2/n*, *P2/c*. The latter three do not resolve the disorder, since the 2-axis is retained. Reduction into *P2<sub>1</sub>/c* and *P1* results in the same type of arrangement, as far as the situation within a single layer is concerned. *P2<sub>1</sub>/c* was selected for deeper analysis. A reduction into *P2<sub>1</sub>/n* or *Cc* also resolves the disorder, again with identical arrangement patterns, and the *Cc* case was selected. A third distinct pattern of hydrogen bonds results from the hypothetical, fully ordered structure in *C2/c*. Here the CH<sub>2</sub> moiety would be positioned on the 2-fold axis, so that the symmetry of the molecule coincides with the site symmetry. However, this orientation of the molecules does not appear within the experimental disorder.

### DFT calculations

Calculations of the lattice energies and energy optimizations of the structures were conducted for these three ordered arrangements within the unit cell of HT-form, as well as for the two existing ordered keto polymorphs of BAc, form I and II (tables 3, 4, S4 supporting information). Their comparison confirms and explains the observed disorder in HT-form.

The optimizations of the experimental forms I and II result in geometries very similar to the experimental ones at 150 K,<sup>7</sup>

**Table 4** Calculations of relative lattice energies for ordered structure models

Structure	H-bond motive	Conformation of molecule		Energy kJ/mol
		experi- mental	energy optimization	
Form I	ladder	envelope	envelope	3.3
Form II	2D layer	envelope & flat	envelope & weak envelope	0
HT-form, <i>Cc</i> subgroup type	2D layer	-	envelope	2.2
HT-form, <i>P2<sub>1</sub>/c</i> subgroup type	ladder	-	envelope	3.6
HT-form, ordered in <i>C2/c</i>	ribbon chains	-	flat	10.0

with calculated unit cell volumes  $\approx 2\%$  too large. The molecule conformations of these two forms are faithfully reproduced. The experimentally flat molecule in form II is optimized to a very weak envelope conformation. This is either an artifact of the calculation, or the very weak envelope conformation is masked by disorder in the real structure. According to the calculations of Lewis *et al.* <sup>7</sup> the stability difference between flat and envelope conformation is only 1.2 kJ/mol, with the latter being more stable. Form II, despite half of its molecules being planar, is still more stable than form I (possessing all enveloped molecules), owing to better geometries for the intermolecular hydrogen bonds. Again, the relative energies are reproduced correctly. Form II is confirmed as the most stable keto-BAc structure.

The *Cc* subgroup type of HT-form is very similar to the crystal structure of form II. In both cases the molecules form the same 2-dimensional layers, in which each molecule is connected to its four neighbors by one hydrogen bond each. The calculations for this structure type give an energy only 2.2 kJ/mol higher than form II. This is in good agreement with the experimental enthalpy of the II  $\rightarrow$  HT transition, 1.33(4) kJ/mol <sup>12</sup> resp. 1.30(4) kJ/mol.<sup>11</sup> Surprisingly, the calculated energy of this HT-form subgroup type is lower than the energy calculated for form I. Since no experimental value that reliably refers to form I could be found, it remains unclear whether this is an artifact of the calculation or represents the real situation. In the *Cc* space group, the angles of the straight hydrogen bonds are not restricted by symmetry. The energy-optimized structure for this model gives values of 160.1° and 126.5°, respectively, for the C=O...N angles along the two directions.

In the *P2<sub>1</sub>/c* subgroup type of HT-form, half of the molecules appear rotated by 180° around the 2-fold axis. The chain of straight hydrogen bonds along the [010] direction is not influenced by this much, as the 2-fold symmetry axis is



parallel to  $\underline{b}$ . The pattern of bent hydrogen bonds is different from the  $Cc$  case, as they both are formed with the same neighbor. Consequently, each molecule is connected by hydrogen bonds only to three of the four direct neighbors within the layer. The resulting pattern of hydrogen bonds is known as the ladder motive<sup>39</sup>. This structure has some similarities with form I, which also consists of ladders. However, while in form I the ladders are arranged at an angle, in the  $P2_1/c$  subgroup type they are parallel, mimicking a layer structure. Due to the experimentally confirmed disorder of HT-form, this ladder motive has to exist at least locally. It appears necessarily at the joint between regions made up from two differently oriented  $Cc$  subgroup types. The energy of this  $P2_1/c$  subgroup type again is 3.6 kJ/mol higher than form II, thus 0.3 kJ/mol higher than form I. However, with an increase of only 1.4 kJ/mol over the  $Cc$  subgroup type, the presence of this motive is not strongly hindered. A disordered structure in  $C2/c$ , in which this arrangement appears locally while the  $Cc$  subgroup type makes up the bulk of the structure, would have a lattice energy only very slightly higher than a fully ordered  $Cc$  subgroup type structure.

In the last arrangement considered herein, ordered in the  $C2/c$  symmetry of HT-form, only bent hydrogen bonds are formed. Each molecule is joined with only two neighbors by two hydrogen bonds each, forming ribbon chains along the  $[101]$  direction. No proper hydrogen bonds appear along the  $[010]$  direction in this structure type. Instead, the presence of short C–H···O contacts along  $[010]$  is a clear indication that this arrangement is energetically not favorable. With lattice energy increased by 10.0 kJ/mol it is not surprising that this type does not contribute to the real structure of HT-form.

## Thermal expansion and phase transition

The II  $\rightarrow$  HT transformation is a reversible first order phase transition. It is accompanied by a discontinuous 1.5(1) % increase in volume, a halving of the unit cell, and a symmetry increase from space group  $P2_1/c$  into space group  $C2/c$ . Narrow two-phase regions exist on heating and on cooling, with temperature ranges larger than the experimentally determined temperature gradient of the furnace. The onset temperature of the II  $\rightarrow$  HT transformation upon heating was found to change little with changes in the heating rate. The first traces of HT-form appear at 233(1) °C and the last reductions of form II happen at 237(1) °C. Note that small fractions of form II (< 5%) persist within the whole phase region of HT-form for long times. The reason for this is unknown. Also, note that the transformation is quite slow. At heating rates above 2 °C/min, HT-form is not formed in significant amounts before decomposition occurs. Irreversible decomposition happens eventually at temperatures above 242(1) °C, at higher temperatures progressively faster. At temperatures below 242(1) °C, HT-form is stable for unlimited times (> 1 week). Note that small amounts of decomposition products appear at temperatures as low as 230 °C.

The HT  $\rightarrow$  II transformation upon cooling depends on the cooling rate. By decreasing the temperature at about 0.5 °/min, undercooled HT-form could be preserved down to

100 °C (figure 7, 8). If HT-form is quenched, most of the compound transforms into form II faster than we could measure. The remaining fraction of undercooled HT-form reverts into form II within 20 hours at ambient conditions. The lattice parameters of this rapidly undercooled HT-form are distinctly different. However, due to the identical symmetry of  $C2/c$  and the very similar pattern of peak intensities it is not justifiable to treat this compound as a separate form.

Within the HT-form region, normal thermal expansion of the lattice occurs. The expansion is moderately strong for the layer stacking distances (0.024(4) %/°C), but not significant inside the layer (0.002(1) %/°C). An interesting feature of HT-form is the value of the monoclinic angle  $\beta$ , which is very close to 90° (for the standard setting).  $\beta$  is temperature dependent, with values > 90° at low temperatures, < 90° at higher temperatures, and crossing over at 225(1) °C, with a value of exactly 90°. This orthorhombic metric is not reflected in the crystal structure. Note that this crossover temperature is below the transformation temperature, so that it can be reached only by cooling down from HT-form.

## Structure-adapted expansion parameters

As discussed previously, a close inspection of the structure reveals a change in the monoclinic axis direction with respect to the direction of straight and bent intermolecular hydrogen bonds. It is tempting to ignore this and treat the HT  $\rightarrow$  II phase transition as a doubling of the  $b$  lattice parameter, as the symmetry transformation  $C2/c$ ,  $a, b, c \rightarrow P2_1/c$ ,  $a, 2b, c$  constitutes a supergroup  $\rightarrow$  subgroup transformation.<sup>40</sup> But a direct comparison of the temperature dependency of the lattice parameters of the two forms makes it clear, that this is not appropriate in this case (figure S5 in supporting information). Instead, a reorientation of the monoclinic axis  $b$  is necessary, resulting in the relations  $a_{HT} - c_{HT}, 2b_{HT}, a_{HT} + c_{HT} \rightarrow b_{II}, a_{II} - c_{II}, a_{II} + c_{II}$ , which destroys the symmetry relation. The structurally equivalent parameters (listed in table S6 of supporting information) resulting from this are:

The stacking distance  $d_1$  of the layers is calculated for both forms as the  $(10\bar{1})$  lattice plane spacing, thus

$$d_1 = \sqrt{\frac{a^2 c^2 \sin^2 \beta}{a^2 + c^2 - 2ac \cos \beta}}.$$

This parameter describes the distance between the individual layers formed by the molecules. The repetition length  $d_2$  along the straight hydrogen bonds is for HT-form the lattice parameter  $b$ , the direction of the 2-fold symmetry axis in this structure. The repetition length  $d_3$  along the bent hydrogen bonds is calculated as half the length of the face diagonal  $a-c$ , thus

$$d_3 = 0.5 \cdot \left( \sqrt{a^2 + c^2} - 2ac \cos \beta \right).$$

For the low-temperature form II, the equations are used *vice versa*, but with half the value of  $b$  used for  $d_3$ .

The thermal expansion of these parameters for both forms is shown in figure 8. All directions exhibit normal behavior within HT-form. This is different for form II, which shows various anomalies in its thermal expansion. When these are

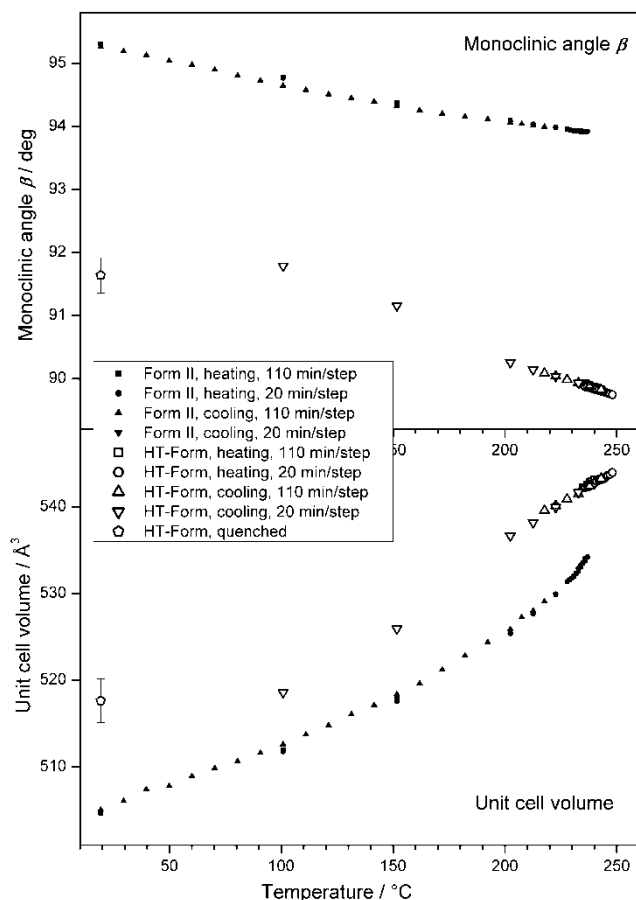


**Fig. 7** Change of the unit cell of HT-form and form II with temperature. Fast cooling can preserve HT-form to lower temperatures for short times. The uncertainty is below the size of the symbols unless error bars are given.

interpreted as changes ultimately leading to the formation of HT-form, the behavior becomes understandable:

### Stacking distance

The stacking distance of the layers  $d_1$  shows normal thermal expansion in form II. Since the expansion of  $d_1$  is much higher than in the other directions it dominates the volume expansion. This is due to the absence of strong bonds holding the layers together. The relative expansion is about 0.025(3) %/°C, approximately the same as in HT-form. Between ambient temperature and the phase transition, this results in a total expansion of the stacking distance of 4 %. The discontinuity at the phase transition adds another 1 %. The driving mechanism of this expansion is straightforward: as the temperature rises, the movement of the molecules increases. Both displacive and rotational movements result in thicker layers and increased stacking distances. Once the thermal energy is high enough to break hydrogen bonds, complete reorientation of the molecules occurs in agreement with the anisotropic motion observed by  $^1\text{H}$  VT MAS. At this point orientational disorder sets in and the structure of form II transforms into HT-form.

### Strong hydrogen bond chains

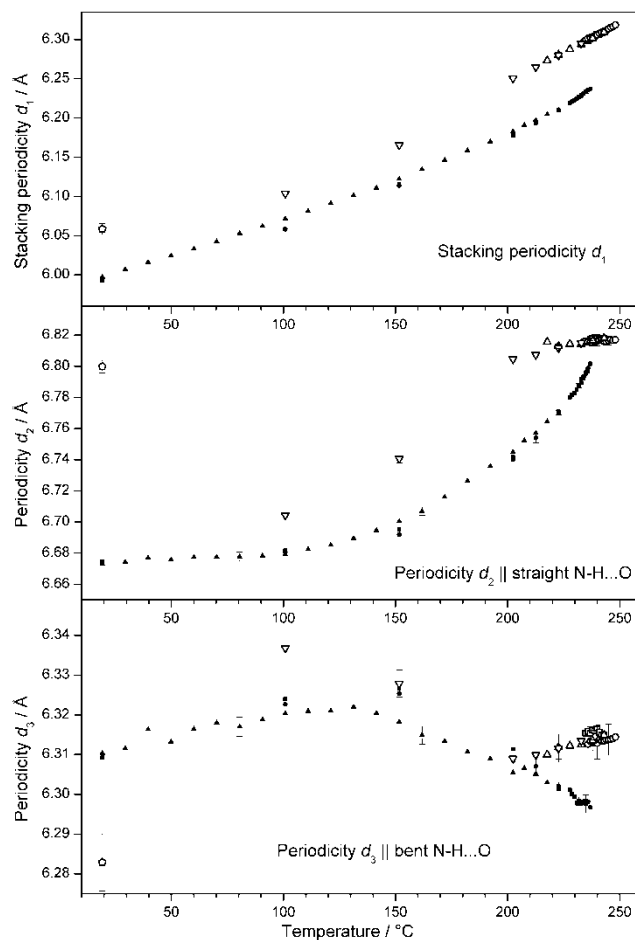


**Fig. 8** Thermal development of structurally comparable distances in HT-form and form II. The uncertainty is below the size of the symbols unless error bars are given. The symbols are given as in figure 7.

The  $d_2$  direction, along the straight hydrogen bonds, shows very different behavior. At low temperatures, below  $\approx 120$  °C, the thermal expansion of form II is very small (0.0014(1) %/°C). The same very small expansion of  $d_2$  is observed within HT-form. This is the result of the intermolecular hydrogen bonds. Above  $\approx 120$  °C, the rate of expansion increases dramatically, reaching 0.037(1) %/°C close to the phase transition. Consequently, the total expansion from ambient temperature to the phase transition is about 2.0(1) %. The discontinuity at the phase transition is not significant for this parameter. If not for the other structural parameters, the transition might be taken for a 2<sup>nd</sup> order phase transition. Overall, this structural direction shows a temperature dependency typical for an order/disorder phase transition<sup>41</sup>. Within the framework of Landau theory<sup>41</sup>, order/disorder phase transitions are associated with the appearance of a new symmetry element in the high-symmetry, disordered (normally the high-temperature) phase. This results in a situation, where the symmetry of a high-temperature structure is a supergroup of the symmetry of the respective low temperature structure.

However, while  $C2/c$  and  $P2_1/c$  have a supergroup-subgroup relation<sup>40</sup>, the reorientation of the monoclinic axis destroys the symmetry relations. It is therefore not trivial, which

symmetry element appearing in HT-form is linked to the lattice expansion behavior. There are two fundamental structural changes. One is the vanishing of the envelope conformation in HT-form due to displacement disorder. But the flat conformation of the molecule is not a function of the symmetry of HT-form, since there are no symmetry elements that prohibit an envelope conformation. The second fundamental change is the appearance of rotational disorder, directly linked to the 2-fold rotational symmetry. Closely connected is the straightening of the hydrogen bonds along the  $d_2$  direction, which in HT-form all have  $N\cdots O=C$  angles of  $180^\circ$ . In form II (150 K) the  $N\cdots O=C$  angle of  $150.5^\circ$  results in a shortening of the hydrogen bond  $N\cdots C$  distance by 2.8 %, which directly translates into an expansion along  $d_2$  upon transformation into HT-form. A fraction of this expansion is counterbalanced by an apparent shortening of the hydrogen bond, from an  $N\cdots O$  distance of  $<2.843>$  Å in form II to 2.781 Å in HT-form.

From the energy optimizations, the  $N\cdots O$  distances of  $<2.840>$  Å in form II are not significantly altered in HT-form, with 2.848 Å in the  $Cc$  subgroup type and 2.838 Å in the  $P2_1/c$  subgroup type. Instead, the straight  $N\cdots O=C$  angles, which were accurately predicted with  $<153.7>^\circ$  for form II, are calculated as not fully stretched in the ordered subgroup types of HT-form ( $160.1^\circ$  in the  $Cc$  type and  $170.5^\circ$  in the  $P2_1/c$  type). This indicates that the observed perfect linearity of the bonds is a result of the disorder masking an imperfect linearity at the local scale.

The nature of the observed disorder gives away the driving force of the structural change. The formation of the disordered structure from the ordered structure of form II requires a rotation of molecules around the  $d_2$  direction. This rotation keeps the hydrogen bonds in this direction intact, while the hydrogen bonds along the lateral  $d_3$  direction are necessarily broken. The preference to break these bent intermolecular hydrogen bonds is unsurprising, as they are weaker<sup>42</sup>. However, dynamic disorder sets in at high temperatures only, as demonstrated conclusively by  $^1H$  VT MAS NMR (figure 4). But even before rotational disorder is achieved, the molecule libration is bound to be preferably around the stronger hydrogen bonds, resulting in a further weakening of the bent hydrogen bonds as temperature and thermal movement increase. This in turn allows the stronger hydrogen bonds along  $d_2$  to take up an energetically even more favorable, nearly linear geometry, at the expense of the lateral hydrogen bonds, which become even more bent. At the phase transition, the disorder and linearity of the straight hydrogen bond become dominant and force a new 2-fold axis along  $d_2$ . With the phase transition, this lattice direction once again adopts normal thermal expansion behavior.

### Weak hydrogen bond chain

The third structural direction  $d_3$ , perpendicular to the other two, lies along the chains of bent hydrogen bonds. At temperatures below  $\approx 120^\circ C$  this length, too, shows typical thermal expansion behavior. The expansion is very small,  $0.0018(2) \text{ } \%/^\circ C$ , similar to  $d_2$ . At higher temperatures,  $d_3$  contracts with increasing temperature, at a rate of  $-0.0035(2) \text{ } \%/^\circ C$ . The resulting sharp bend in the lattice parameter curve

allows the precise determination of the onset temperature of thermal libration as  $125(5)^\circ C$ . Within HT-form, the parameter once again adopts normal thermal expansion, with a rate of  $0.0019(3) \text{ } \%/^\circ C$ , not significantly different from the low-temperature range of form II. Over the whole temperature range of both phases, the total expansion in this direction is only 0.3 %. This is even more surprising if one considers the fact the  $N\cdots O$  distance in the respective hydrogen bonds increases from  $<2.838>$  Å in form II to 3.104 Å in HT-form, which should result in an expansion of 4 %. As these changes in the hydrogen bond geometry are reflected in the energy-optimized structures, they are not a direct result of librational shortening, since disorder effects are not considered in *ab initio* models. Also, the  $C=O\cdots N$  angles do not change very much for these bonds, from  $<133.1>^\circ$  in form II to  $128.1^\circ$  in HT-form. The parameter responsible for the contraction is the straightening-up of the molecules, as their straight hydrogen bond comes to lie parallel to  $d_2$ . This tilts the  $C=O$  bonds involved in the bent hydrogen bonds away from the  $d_3$  direction. The hydrogen bonds itself are tilted by the same magnitude, in order to preserve the straight  $N-H\cdots O$  angle. In total, all interatomic vectors that define the length of  $d_3$  are tilted away from this direction, from an angle of  $20^\circ$  in form II to  $26^\circ$  in HT-form. The corresponding geometric shortening of the  $d_3$  direction is -4 %, exactly enough to counterbalance the increase of the hydrogen bond length. The changes in the thermal expansion in the  $d_2$  and  $d_3$  directions are directly linked by this mechanism.

### Quenching

On a side note, when quenching HT-form, it behaves different from slower cooling. The unit cell of the quenched structure preserves the geometry of HT-form. This is especially pronounced in the high value of  $d_2$  and the low value of  $d_3$  (figure 8), which are in good agreement with the extrapolated thermal expansion of HT-form. The presence of orientational disorder stabilizes the structure of HT-form. An ordering would require the breaking of hydrogen bonds, which is hindered at lower temperatures. If the sample is cooled down slower,  $d_2$  and  $d_3$  mimic the behavior of form II. This indicates that the local structure within the layers already has reverted into the low-temperature conformation. The monoclinic angle, the orientation of the monoclinic axis, and the absence of the doubling of the  $d_3$  direction still reflect HT-form. For these parameters to revert to the ones of form II, the arrangement of the layers has to change.

### Summary

The high-temperature form of barbituric acid is formed by rotational disorder of the molecules. This disorder is dynamic on the NMR time scale, as observed by  $^{13}C$  and  $^1H$  VT MAS spectra, which highlight the anisotropic character of the rotation. The necessary rotation of the molecules breaks only the weaker hydrogen bonds, and leaves intact the fundamental layer structure of the compound. Ordered subgroup structures of HT-form have lattice energies that are only slightly higher than form II. However, due to the similar arrangement of the molecules within the crystal structures of HT-form and form

II, only short-term preservation of HT-form is possible at ambient temperatures. The unusual behavior of the thermal expansion of form II can only be understood in light of the structure of HT-form. Conversely, the proper relation between the two structures only becomes obvious through the analysis of thermal expansion.

## Acknowledgements

This work is partly based on experiments performed at the Swiss spallation neutron source SINQ, Paul Scherrer Institute, Villigen, Switzerland. Financial support from Sandoz GmbH is gratefully acknowledged by DMT. MRC is indebted with Prof. L. Marchese and Dr. G. Paul for allowing using the NMR instrument in Alessandria. Insightful NMR discussions with Profs P. Hodgkinson and S. Caldarelli are gratefully acknowledged. Also, we are grateful to Prof. C. Nervi for performing NMR calculation on BAc.

## References

- 1 A. von Baeyer, *Ann. Chem. Pharm.* 1863, **127**, 199-236.
- 2 A. Slaczka and J. Lubczak, *J. Appl. Polym. Sci.* 2007, **106**, 4067-4074.
- 3 D. Thetford, A. P. Chorlton and J. Hardman, *Dyes Pigments* 2003, **59**, 185-191.
- 4 A. V. Kulinich, N. A. Derevyanko and A. A. Ishchenko, *Russ. J. Gen. Chem.* 2006, **76**, 1441-1457.
- 5 M. Tishler, K. Pfister, R. D. Babson, K. Ladenburg and A. J. Fleming, *J. Am. Chem. Soc.* 1947, **69**, 1487-1492.
- 6 W. Bolton, *Acta Crystallogr. B* 1963, **16**, 166-173.
- 7 T. C. Lewis, D. A. Tocher and S. L. Price, *Cryst. Growth Des.* 2004, **4**, 979-987.
- 8 D. Braga, M. Cadoni, F. Grepioni, L. Maini and K. Rubini, *Cryst. Eng. Comm.* 2006, **8**, 756-763.
- 9 M. R. Chierotti, R. Gobetto, L. Pellegrino, L. Milone and P. Venturello, *Cryst. Growth Des.* 2008, **8**, 1454-1457.
- 10 M. U. Schmidt, J. Brüning, J. Glönnemann, M. W. Hützler, P. Mörschel, S. N. Ivashevskaya, J. van de Streek, D. Braga, L. Maini, M. R. Chierotti and R. Gobetto, *Angew. Chem. Int. ed.* 2011, **50**, 7924-7926.
- 11 M. V. Roux, M. Temprado, R. Notario, C. Foces-Foces, V. N. Emelyanenko and S. P. Verevkin, *J. Phys. Chem. A* 2008, **112**, 7455-7465.
- 12 N. Zencirci, E. Gstrein, Ch. Langes and U. J. Griesser, *Thermochimica Acta* 2009, **485**, 33-42.
- 13 P. Fischer, G. Frey, M. Koch, M. Könnicke, V. Pomjakushin, J. Schefer, R. Thut, N. Schlumpf, R. Bürge, U. Greuter, S. Bondt and E. Berruyer, *Physica B* 2000, **276**, 146-147.
- 14 STOE, *WinXPow 2.10*, unpublished (2004).
- 15 R. Shirley, *The Crysfire 2002 System for Automatic Powder Indexing*, The Lattice Press: Guildford, Surrey, England (2002).
- 16 J. Laugier and B. Bochu, *LMGP-Suite of Programs for the interpretation of X-ray Experiments*, ENSP/Laboratoire des Matériaux et du Génie Physique, BP 46. 38042 Saint Martin d'Hères, France (2004).
- 17 V. Favre-Nicolin and R. Černý, *J. Appl. Cryst.* 2002, **35**, 734-743.
- 18 J. Rodríguez-Carvajal, *Physica B* 1993, **192**, 55-69.
- 19 V. Schomaker and K. N. Treublood, *Acta Cryst. B* 1968, **24**, 63-76.
- 20 J.-F. Bérar and P. Lelann, *J. Appl. Crystallog.* 1991, **24**, 1-5.
- 21 K. Eichele and R. E. Wasylshen, *HBA 1.6*, Dalhousie University and Universität Tübingen, (2010).
- 22 J. Herzfeld and A. E. Berger, *J. Chem. Phys.* 1980, **73**, 6021-6030.
- 23 M. R. Chierotti, L. Garlaschelli, R. Gobetto, C. Nervi, G. Peli, A. Sironi and R. Della Pergola, *Eur. J. Inorg. Chem.* 2007, 3477-3483.
- 24 M. J. Frisch, G. W. Trucks, H. B. Schlegel, G. E. Scuseria, M. A. Robb, J. R. Cheeseman, G. Scalmani, V. Barone, B. Mennucci, G. A. Petersson, H. Nakatsuji, M. Caricato, X. Li, H. P. Hratchian, A. F. Izmaylov, J. Bloino, G. Zheng, J. L. Sonnenberg, M. Hada, M. Ehara, K. Toyota, R. Fukuda, J. Hasegawa, M. Ishida, T. Nakajima, Y. Honda, O. Kitao, H. Nakai, T. Vreven, J. A. Jr. Montgomery, J. E. Peralta, F. Ogliaro, M. Bearpark, J. J. Heyd, E. Brothers, K. N. Kudin, V. N. Staroverov, R. Kobayashi, J. Normand, K. Raghavachari, A. Rendell, J. C. Burant, S. S. Iyengar, J. Tomasi, M. Cossi, N. Rega, J. M. Millam, M. Klene, J. E. Knox, J. B. Cross, V. Bakken, C. Adamo, J. Jaramillo, R. Gomperts, R. E. Stratmann, O. Yazyev, A. J. Austin, R. Cammi, C. Pomelli, J. W. Ochterski, R. L. Martin, K. Morokuma, V. G. Zakrzewski, G. A. Voth, P. Salvador, J. J. Dannenberg, S. Dapprich, A. D. Daniels, O. Farkas, J. B. Foresman, J. V. Ortiz, J. Cioslowski and D. J. Fox, *Gaussian 09, Revision A.02*, Gaussian, Inc., Wallingford CT (2009).
- 25 M. A. Neumann, *Program GRACE*, see <http://www.avmatsim.eu>
- 26 G. Kresse and J. Furthmüller, *Comput. Mater. Sci.* 1996, **6**, 15-50.
- 27 G. Kresse and J. Hafner, *Phys. Rev. B* 1993, **47**, 558-561.
- 28 G. Kresse and D. Joubert, *Phys. Rev. B* 1999, **59**, 1758-1775.
- 29 A.D. Becke, *J. Chem. Phys.* 1988, **88**, 3098-3100.
- 30 C. Lee, W. Yang and R. G. Parr, *Phys. Rev. B* 1988, **37**, 785-789.
- 31 S. Grimme, J. Antony, S. Ehrlich and H. Krieg, *J. Chem. Phys.* 2010, **132**, 154104. DOI:10.1063/1.3382344.
- 32 M. R. Chierotti, L. Ferrero, N. Garino, R. Gobetto, L. Pellegrino, D. Braga, F. Grepioni and L. Maini, *Chem. Eur. J.* 2010, **16**, 4347-4358.
- 33 M. R. Chierotti and R. Gobetto, *Eur. J. Inorg. Chem.* 2009, 2581-2597.
- 34 S. Pelloni, R. Carion, V. Liégeois and P. Lazzeretti, *J. Comput. Chem.* 2011, **32**, 1599-1611.
- 35 L. Yao, A. Grishaev, G. Cornilescu and A. Bax, *J. Am. Chem. Soc.* 2010, **132**, 10866-10875.
- 36 A. M. Kantola, P. Lantto, J. Vaaraab and J. Jokisaari, *Phys. Chem. Chem. Phys.* 2010, **12**, 2679-2692.
- 37 H. Saitô, I. Ando and A. Ramamoorthy, *Progr. Nucl. Magn. Reson. Spectr.* 2010, **57**, 181-228.
- 38 V.F. Sears, *Scattering lengths for neutrons, International tables for crystallography, Vol. C*, Third edition, chapter 4.4.4, Kluwer Academic Publishers, Dordrecht/Boston/London (2004).
- 39 A. M. Beatty, *Coord. Chem. Rev.* 2003, **246**, 131-143.
- 40 H. T. Stokes and D. M. Hatch, *Isotropy subgroups of the 230 crystallographic space groups*. World Scientific, Singapore (1988).
- 41 J.-C. Tolédano and P. Tolédano, *The Landau theory of phase transitions*, World scientific lecture notes in physics, Vol. 3, World Scientific Publishing Co. Pte, Ltd., Singapore (1987).
- 42 R. Taylor, O. Kennard and W. Versichel, *Acta Cryst. B* 1984, **40**, 280-288.